Evaluation of coal longwall caving characteristics using an innovative UDEC Trigon approach

Fuqiang Gao [a,*], Doug Stead [a], John Coggan [b]

[a] Engineering Geology and Resource Geotechnics Group, Simon Fraser University, Burnaby, BC, Canada

[b] Camborne School of Mines, University of Exeter, United Kingdom

Abstract: The paper presents an innovative numerical approach to simulate progressive caving of strata above a longwall coal mining panel. A proposed Trigon logic is incorporated within UDEC to successfully capture the progressive caving of strata which is characterized by fracture generation and subsequent propagation. A new damage index, D, is proposed that can quantify regions of both compressive shear and tensile failure within the modelled longwall. Many features of progressive caving are reproduced in the model and found to fit reasonably well with field observations taken from a case study in the Ruhr coalfield. The modelling study reveals that compressive shear failure, rather than tensile failure, is the dominant failure mechanism in the caved strata above the mined-out area. The immediate roof beds act like beams and can collapse in beam bending when vertical stress is dominant or in beam shear fracture when horizontal stress is dominant. The proposed numerical approach can be used to guide the design of longwall panel layout and rock support mechanisms.

Keywords: longwall mining; numerical simulation; discrete element; fracture; damage

1 Introduction

Longwall mining is a widely used underground mining method for the extraction of relatively thick, sub-horizontal and uniform coal seams. After mining of the coal seam, the panel roof strata above the mined-out area or goaf will be destressed. With continued face advance, the immediate roof will collapse and cave into the goaf area, and the disturbed roof strata gradually extends upwards. Three zones of disturbance may be identified above the goaf, as illustrated in Fig. 1; a caved zone, a fractured zone and a continuous deformation zone, in ascending order from the roofline [1]. The extent of each zone depends on the geological and geotechnical conditions of the overburden strata including the mechanical properties of the rock, in situ stress, the thickness of the coal seam and immediate strata, and the type and nature of the strata [2]. Understanding the failure mechanism associated with the progressive caving of

strata is very important for predicting ground subsidence, roadway, face support and mine layout design.

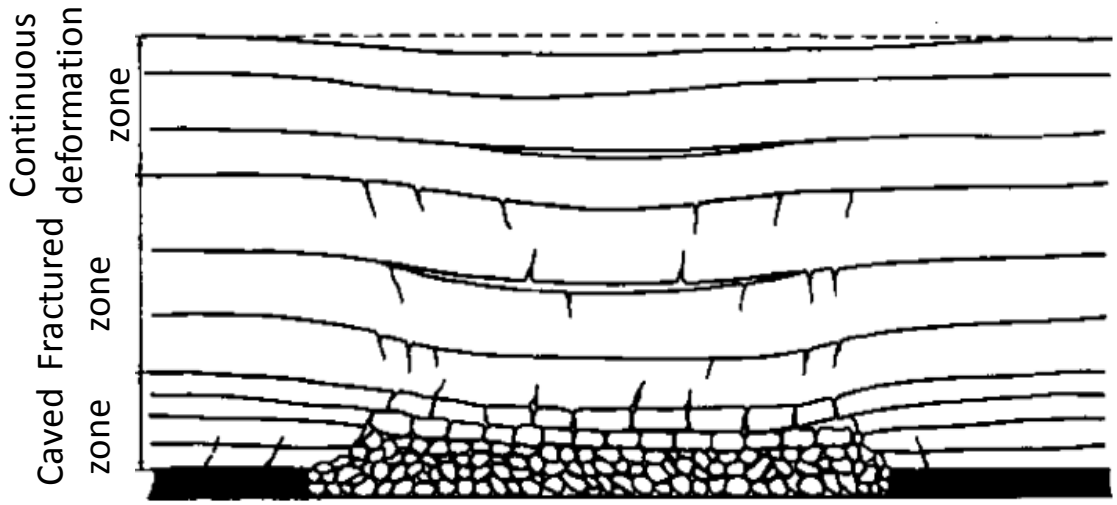

Fig. 1 Disturbed zones due to excavation of a panel in longwall mining (after [1]).

Common approaches for studying the progressive caving of strata include empirical, physical modelling, and numerical modelling methods. Empirical methods suffer from a number of simplifications and are limited when dealing with complex geological mining conditions. Physical models can provide a realistic simulation of the caving process but can be very expensive and time-consuming [3,4].

Numerical modelling is a promising and effective tool for the simulation of progressive caving of strata caused by extraction of a longwall panel. Numerical methods can be classified into continuum methods including BEM (Boundary Element Method), FEM (Finite Element Method), FDM (Finite Difference Method), and discontinuum methods including DEM (Distinct Element Method), DDA (Discontinuous Deformation Analysis) and hybrid FEM/DEM and FDM/DEM. Continuum methods have been widely used for simulating longwall mining [4–12]. There are two major limitations in longwall modelling simulation associated with continuous methods. The first is that the generation and propagation of fractures cannot be explicitly captured and thus the caved zone and fractured zone are unable to be identified directly, but must be determined through assumptions based on displacement, plastic shear strain. The second is that it is difficult to directly incorporate pre-existing discontinuities including bedding planes and cross joints in a continuum model. Discontinuum methods may therefore be considered more appropriate for simulating progressive caving of strata caused by longwall

mining. Coulthard [13], for example, applied the Universal Distinct Element Code (UDEC) [14] to investigate longwall coal mining induced subsidence. In his models, the horizontal bedding planes were given appropriate properties and allowed to open or slip according to the stresses developed. The sub-vertical joints were initially given intact rock shear and tensile strength but due to the stresses induced could mimic the cracks generated and propagating through the strata. Coulthard suggested that UDEC models provide a closer approximation to the real mechanics of the system than a continuum model [13]. UDEC has also been used to simulate the longwall top coal caving method [15–18]. A limitation in these models was that fractures could only develop along pre-existing discontinuities including persistent bedding planes and cross joints.

The proposed UDEC Trigon approach is used in this paper to create a longwall model in which the roof is simulated as an assembly of triangular blocks bonded via contacts. Pre-existing fractures, including bedding planes and cross joints, have been incorporated in the model. Using this approach, the suggested limitations mentioned above are overcome. The modelling results have been compared against field observations. The effects of a soft immediate roof, bedding plane thickness and high horizontal stress on the progressive caving of the strata are investigated.

2 Discrete element modelling of a longwall

2.1 Geology

The current UDEC Trigon modelling study is based on a published longwall panel case study at the German Ruhr mining district [19]. The longwall panel is located at a depth of approximately 1100 m. The mined coal seam has a height of 2-2.5 m. The width of the longwall is 300 m and its length 2000 m. The immediate roof comprises a massive coarse sandstone with an average thickness of 19 m and an intact compressive strength of 112 MPa. It is overlain by a 2 m strong fine-grained sandstone/siltstone layer with an intact compressive strength of 125 MPa. Above that is a 2 m weak siltstone layer of 20 MPa compressive strength. Fig. 2 shows the lithology of the longwall as well as some important geotechnical parameters.

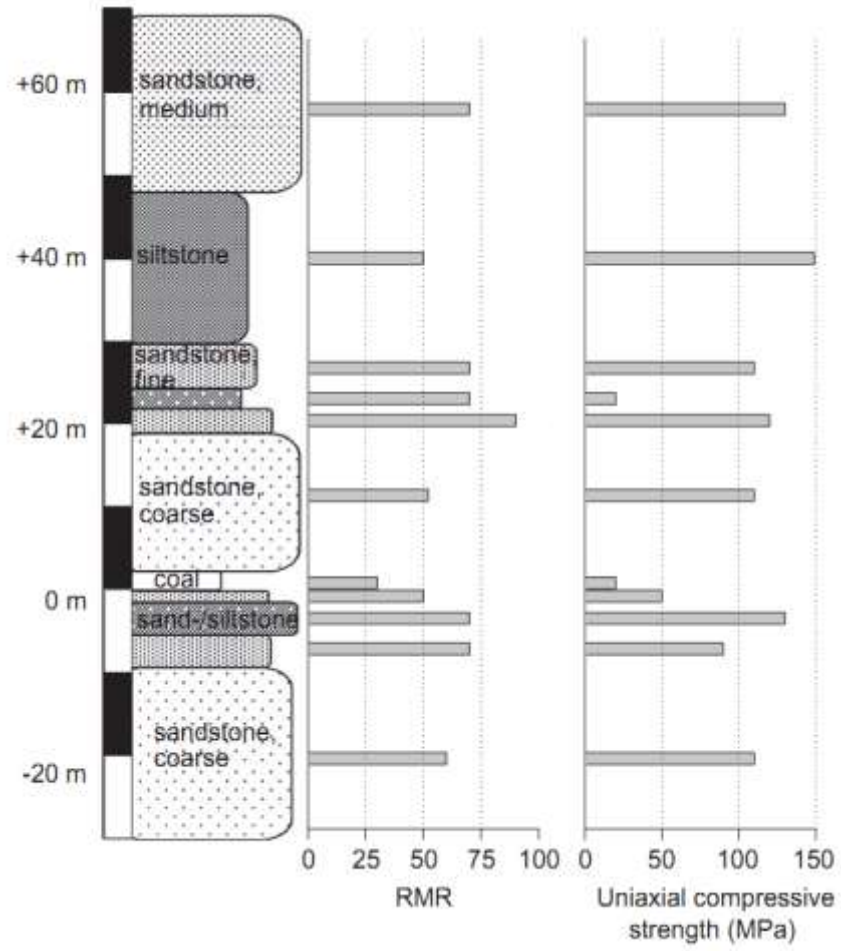

Fig. 2 Lithology and geotechnical parameters (after [19]).

The in situ stresses were extrapolated from nearby stress measurements and are assumed to be as follows: vertical stress $\sigma_v = 27\text{-}29$ MPa, major horizontal stress $\sigma_H = 28\text{-}39$ MPa, and minor horizontal stress $\sigma_h = 15\text{-}19$ MPa [19].

2.2 Rock properties

The intact rock and rock mass properties of the Coal Measure rocks including RMR, mi and σ_{ci} were obtained directly from [19]. The rock mass properties were evaluated using the modified approach of [20].

The *GSI*, σ_{ci}, and m_i were then input into RocLab to calculate rock mass properties [21]. The application option was selected as 'tunnels' with a depth of 1100 m. The intact rock properties and the calculated rock mass properties are illustrated in Table 1.

Table 1 Mechanical parameters of Coal Measures rocks (After Alber et al., 2009).

Bed-No.	Lithology	Thickness (m)	E (GPa)	GSI	σ_{ci} (MPa)	mi	E_m (GPa)	σ_m (MPa)	c (MPa)	Phi (°)	σ_t (MPa)
H6	Sst, m	18	23	69	128	2.2	16.42	22.8	6.2	28.7	2.1
H5	Slt	18	22	45	108	34.7	4.9	31.2	4.2	46.3	2.1
H4	Sst, f	6	20	63	108	7.0	11.8	21.9	4.1	37.7	1.7
H3	Slt	2	10	70	20	5.5	7.3	4.6	1.9	25	0.6
H2	Sst, f/Slt	2	26	86	125	16.4	24.2	67.6	9.8	51.4	5.6
H1	Sst, c	19	22	47	112	17.0	5.6	23.7	3.6	41.2	1.6
Seam A	Coal	2.5	5	32	15	4.5	0.5	1.2	0.75	30	0.3
L1	Sst, f	1	20	43	50	16.0	3.9	9.4	2.4	33.1	0.9
L2	Sst/Sltst.	5	27	70	125	17.0	19.8	43.5	5.8	48.3	3.0
L3	Sst, f	3	23	65	95	17.0	14.5	29.4	4.6	45	2.2
L4	Sst/Sltst	24	25	60	110	9.0	13	22.9	3.9	39.3	1.6

Sst = sandstone, Slt = siltstone, f = fine grained, m = medium grained, c = coarse grained, E = Young's modulus, σ_{ci} = intact compressive strength, σ_m = rock mass compressive strength, E_M = rock mass modulus, c = cohesion, Phi = internal frictional angle, σ_t = rock mass tensile strength.

Note that the rock mass properties cannot be directly assigned to the model. In the UDEC Trigon model, the micro properties of the contacts and blocks control the mechanical behaviour of the material and must be calibrated to the material properties. For each rock mass, the micro properties of the triangular blocks and contacts were calibrated to its rock mass properties. The calibrated properties are given in Table 2.

Table 2 Calculated mechanical properties used in the UDEC Trigon model.

Lithology	Matrix properties		Contact properties				
	Density ($kg \cdot m^{-3}$)	E* (GPa)	k_{n*} (GPa/m)	k_{s*} (GPa/m)	Cohesion (MPa)	Friction (°)	Tensile strength (MPa)
H6	2600	16.4	78.8	27.6	7.8	15.5	6.4
H5	2600	4.9	23.5	8.2	5.3	25.0	3.2
H4	2600	11.8	56.6	19.8	5.1	20.4	2.6
H3	2600	7.3	35.0	12.3	2.4	13.5	0.9
H2	2600	24.2	116.2	40.7	12.3	30.0	8.5
H1	2500	5.6	26.9	9.4	4.5	22.3	2.4
Seam A	1400	2.0	9.6	3.4	16.2	0.9	0.5
L1	2600	3.9	18.7	6.6	3.0	17.9	1.4
L2	2600	19.8	95.0	33.3	7.3	26.1	4.5
L3	2600	14.5	69.6	24.4	5.8	24.3	3.3
L4	2600	13.0	62.4	21.8	4.9	21.2	2.4

2.3 UDEC Trigon

A two dimensional discrete element model has been developed to simulate progressive caving of strata due to longwall mining. A rock is represented as an assembly of triangular blocks bonded together through the contacts between them. Each block is made elastic by dividing it into triangular finite difference zone and hence does not fail. Failure can only occur along the contacts through shear or tension, depending on the stress state and the properties of the contact surface. In the normal direction of a contact, the stress-displacement relation is assumed to be linear and governed by the stiffness k_n such that [14]

$$\Delta\sigma_n = -k_n \Delta u_n \qquad (1)$$

Where $\Delta\sigma_n$ is the effective normal stress increment and Δu_n is normal displacement increment. There is a limiting tensile strength, T, for the contact. If the tensile strength is exceeded, then $\sigma_n = 0$.

In the shear direction, the response is governed by a constant shear stiffness. The shear stress, τ_s, is determined by a combination of contact micro properties, cohesive (C) and frictional (ϕ). Thus, if

$$\left|\tau_s\right| \le C + \sigma_n \tan\phi = \tau_{\max} \quad (2)$$

then

$$\Delta\tau_s = -k_s \Delta u_s^e \quad (3)$$

or else, if

$$\left|\tau_s\right| \ge \tau_{\max} \quad (4)$$

then

$$\tau_s = sign(\Delta u_s^e)\tau_{\max} \quad (5)$$

where Δu_s^e is the elastic component of the incremental shear displacement and Δu_s is the total incremental shear displacement. The *sign* here is a mathematical symbol indicating that $\tau_s = \tau_{\max}$ if Δu_s^e is positive and $\tau_s = -\tau_{\max}$ if Δu_s^e is negative.

This modelling approach is proposed as ‘Trigon logic’ and has been implemented using UDEC Voronoi. With this logic, fracturing can be realistically simulated.

2.4 Model construction

A longwall model has been created using the above UDEC Trigon logic, Fig. 3. The model is 400 m long and 280.5 m high and simulates the longitudinal section through the initial stage of panel extraction. To improve computational efficiency, only the roof where caving occurs is discretized into triangular blocks. The block size is 2.0 m which is considered to be sufficiently small to simulate roof caving. The coal seam and the floor are discretized into coarse rectangular blocks. The bedding planes between layers have been simulated by horizontal persistent joints. In addition, pre-existing discontinuities including bedding planes and cross joints have been incorporated within the roof (Fig. 3). In this preliminary modelling study the cohesion and tensile strength of these pre-existing discontinuities are assumed to be zero and the friction angle assumed to be 30 degree.

Horizontal displacement has been restrained on the left and right model boundaries and both vertical and horizontal displacement fixed in the base. An in situ stress state with $\sigma_v = 27$ MPa, $\sigma_H = 39$ MP and $\sigma_h = 18$ MPa was imposed in the model. σ_h is parallel to the longwall advance direction and σ_H is perpendicular to the longwall advance direction. A vertical stress of 27 MPa has been applied on the top boundary equal to the overburden weight.

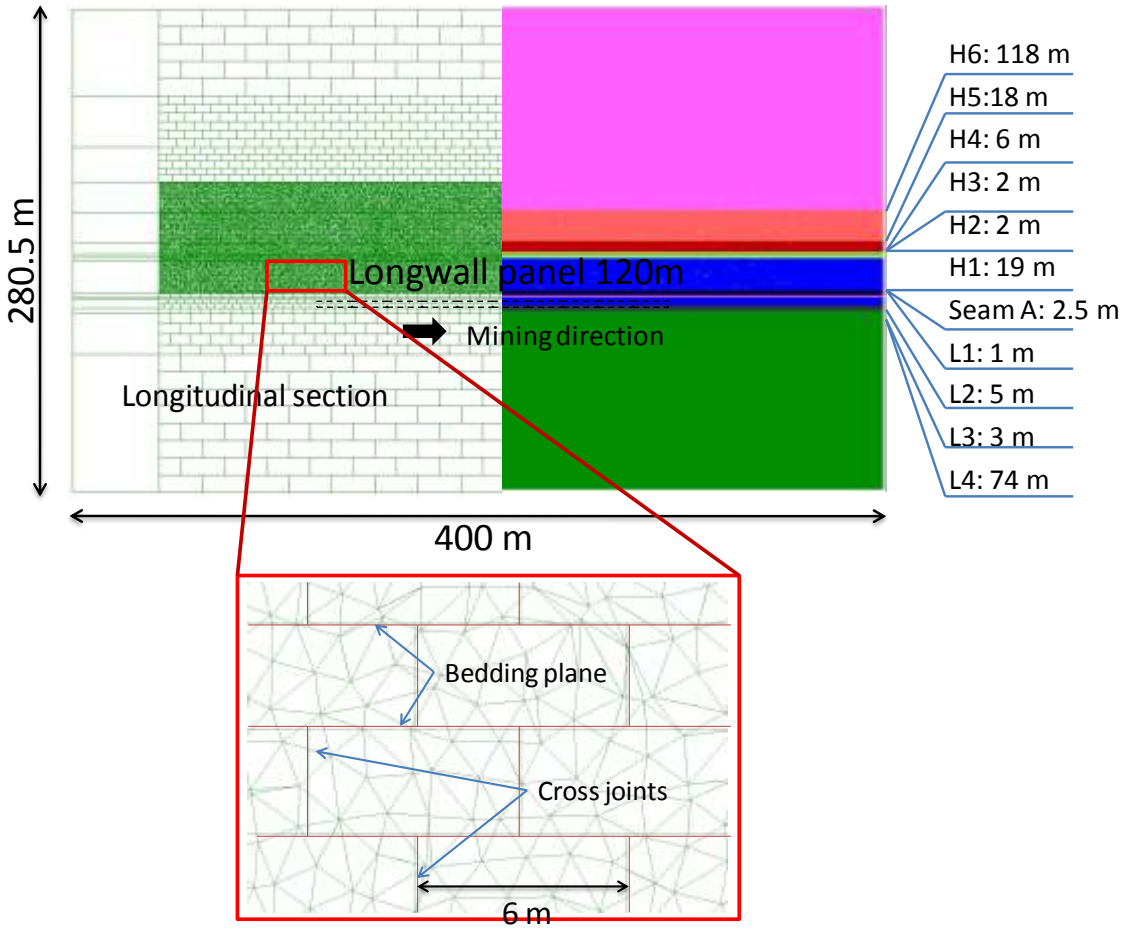

Fig. 3 ***Configuration of longwall model using UDEC Trigon logic.***

2.5 Monitoring approach

To obtain a thorough understanding of the caving process, the mechanical behaviour of the modelled roof has been monitored in detail with longwall face advance. Firstly, the roof is divided into several monitoring regions according to the stratigraphy, Fig. 4. Additional monitoring regions are setup with more in the immediate roof and less in the upper layers. For each region, the shear and tension cracks generated with longwall face advance have been monitored through a custom-developed FISH function. Horizontal and vertical stresses in the central zone element of each monitoring region have also been monitored.

The advance of the longwall, from the left side to the right side of the model, is simulated using a stepwise excavation; each stage involving a 12 m advance and reflecting three days of longwall mining [19]. For each stage, sufficient time steps (15 000*n where n is the stage number) have been run to relieve stress and to allow the roof to cave.

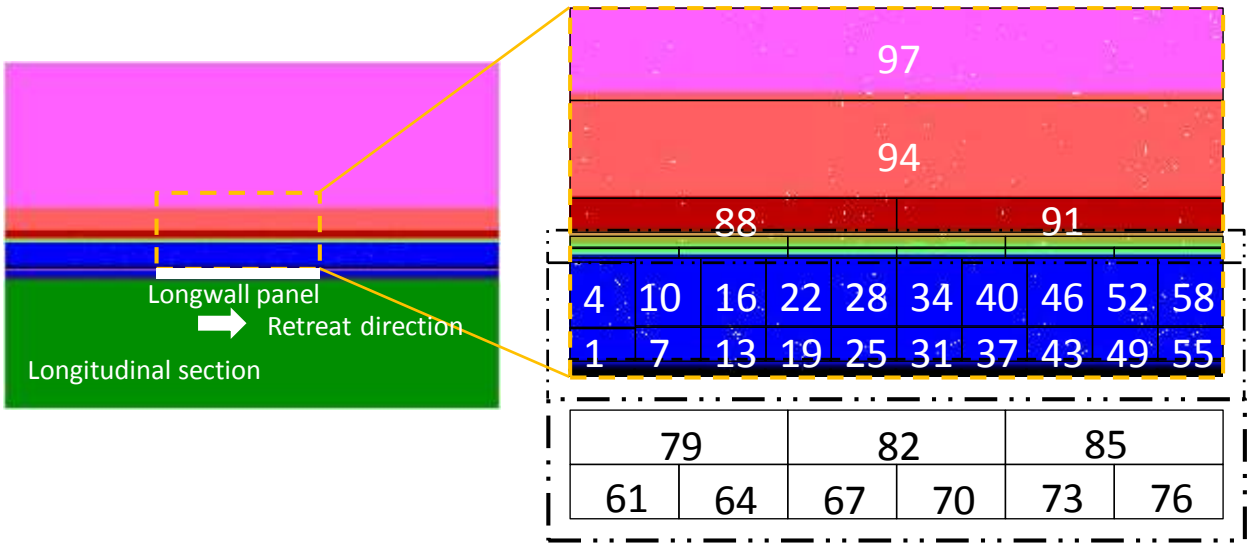

Fig. 4 ***Monitoring regions in longwall model.***

3 Numerical simulation results

3.1 Progressive caving caused by longwall mining

Fig. 5 shows the simulated plots of progressive roof failure. At the first stage, due to the extraction of coal seam, the immediate roof above the mined panel is unsupported and hence is allowed to deform and fail. Few fractures are generated in the immediate roof, Fig. 5 (a). The immediate roof is highly competent so no collapse and caving are observed and the roof remains stable in this stage of the modelled excavation. As the face advances, however, more fractures are generated and extend deeper (approximately 10 m) into the roof (Fig. 5(b)). The immediate roof behaves like a beam and starts to bend downward at the third stage of excavation, at a face advance of 36 m. Bed separation initiates at this stage. Shear fractures form in the H3 layer, while no fracturing occurs in the H2 layer due to its higher strength. As the face continues to advance, fractures extend deeper into the roof, with bed separation reaching a height of approximately 19 m (Fig. 5(c)). When the face has advanced 48 m, fractures extend within the H3 layer (Fig. 5(d)). With a modelled face advance of 60 m, the first layer of the immediate roof collapses and caves into the goaf area (Fig. 5 (e)), followed by the second layer (Fig. 5 (f)). Fractures extend approximately 40 m into the roof. A zoomed-in plot of the fracture pattern at this stage is shown in Fig. 6. Three distinct zones, the caved zone, the fractured zone and a continuous zone are realistically captured within the model. As the face continues to advance the immediate roof further caves and bed separation and fractures extend toward the

top of the model. Generally, the model exhibits a beam bending failure pattern in the immediate roof, in agreement with the field observations and 2D finite element modeling results [19].

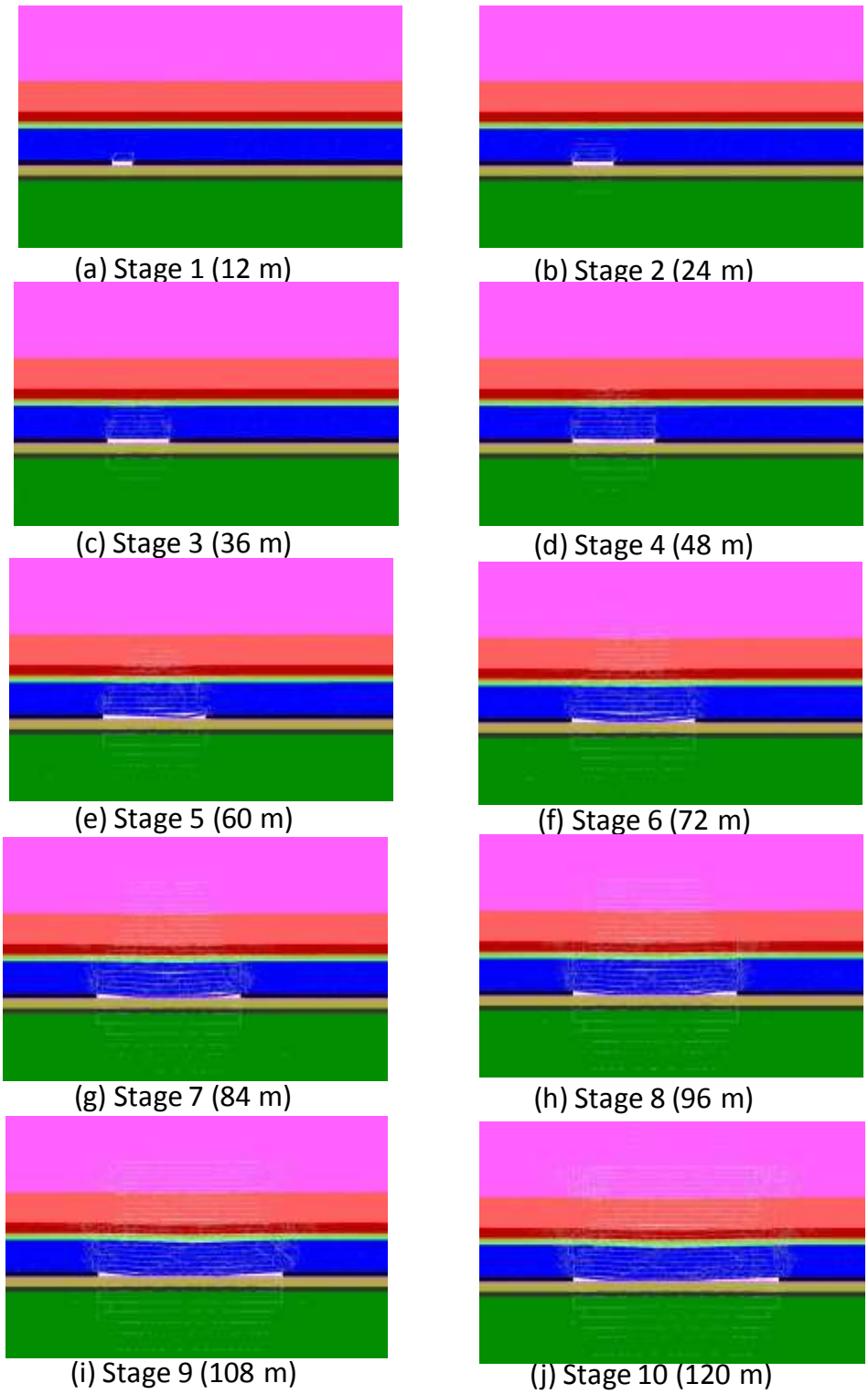

Fig. 5 ***Simulated progressive caving of the strata due to the extraction of a longwall coal panel.***

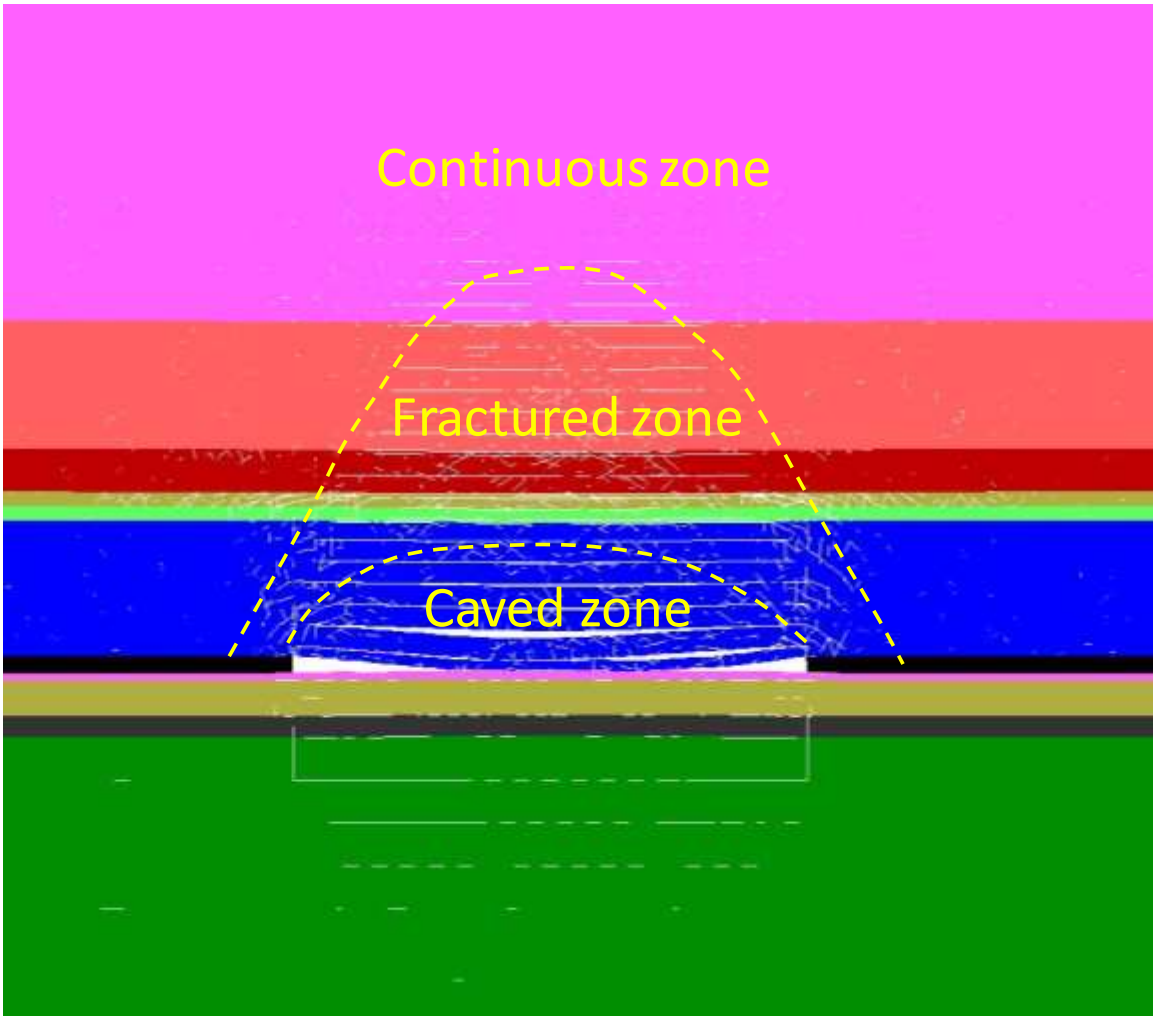

Fig. 6 ***Simulated caved zone, fractured zone and continuous zone due to extraction of a panel in longwall mining.***

3.2 Stress changes

The extraction of the coal seam and caving of the roof causes stress redistribution around the opening. Knowledge of the stress change is very important in understanding the caving process, and in designing both face and roadway support. The vertical stress distribution around the longwall panel at different mining stages is shown in Fig. 7. The extraction of coal results in stress concentration in the un-mined coal and in the roof adjacent to the opening. The vertical stress in the immediate roof and floor is relieved. The area of both the stress concentration and stress relief zones increases with face advance. When the face has advanced far enough (72 m at stage 6), the immediate roof collapses and caves, resulting in closure of the mined void. It should be noted that the rear and front abutment stress continues to increases after the immediate roof collapses. The front and rear abutment stresses continue

to increases as the face advance. Stress redistribution at face-ends and more complex three-dimensional effects of strata behaviour and caving characteristics are not simulated due the two-dimensioanl nature of the model geometry.

The modelled stress changes are analyzed in detail by plotting the vertical stress at selected monitoring points with face advance. The monitored vertical stress at 12 points in the immediate roof is shown in Fig. 8. These 12 points can be considered as representing three different types of behaviour according to the observed patterns in stress change. The first type involves P1 and P12, which are located in the immediate roof above the un-mined coal. At P1, the simulated vertical stress increases gradually as the face advances away and reaches a peak stress of 60.0 MPa when the distance to the face exceeds 84 m. Beyond this, no obvious stress change is observed with further face advance, indicating an eventual stress equilibrium condition at P1. At P12, the vertical stress starts to increase when the face is approximately 84 m away from the monitoring point. These stress change patterns, at P1 and P12, indicate that mining-induced stress changes can be observed up to 80-90 m ahead of the modelled longwall panel. The second type of behaviour involves P5 and P8 which are located in the central part of the immediate roof. At these two points, the vertical stress change is characterized by three distinct stages: a significant stress increase as the face approaches, a sharp stress drop to zero as the face passes, and a gradual increase as the roof caves and compacts. The third type of observed behaviour involves P2 to P4, P6, P7 and P9 to P11. At these points, the vertical stress initially increases as the face approaches and then sharply drops to zero after the face passes. At P11, the vertical stress starts to increase when the face is approximately 84 m away, confirming that the influence of the mining-induced stress changes can reach up to 80-90 m in front of the face. It should be noted that the monitored peak vertical stress increases from 35.5 MPa at P3 to 61.6 MPa at P11, indicating that the front abutment stress increases as the face advances.

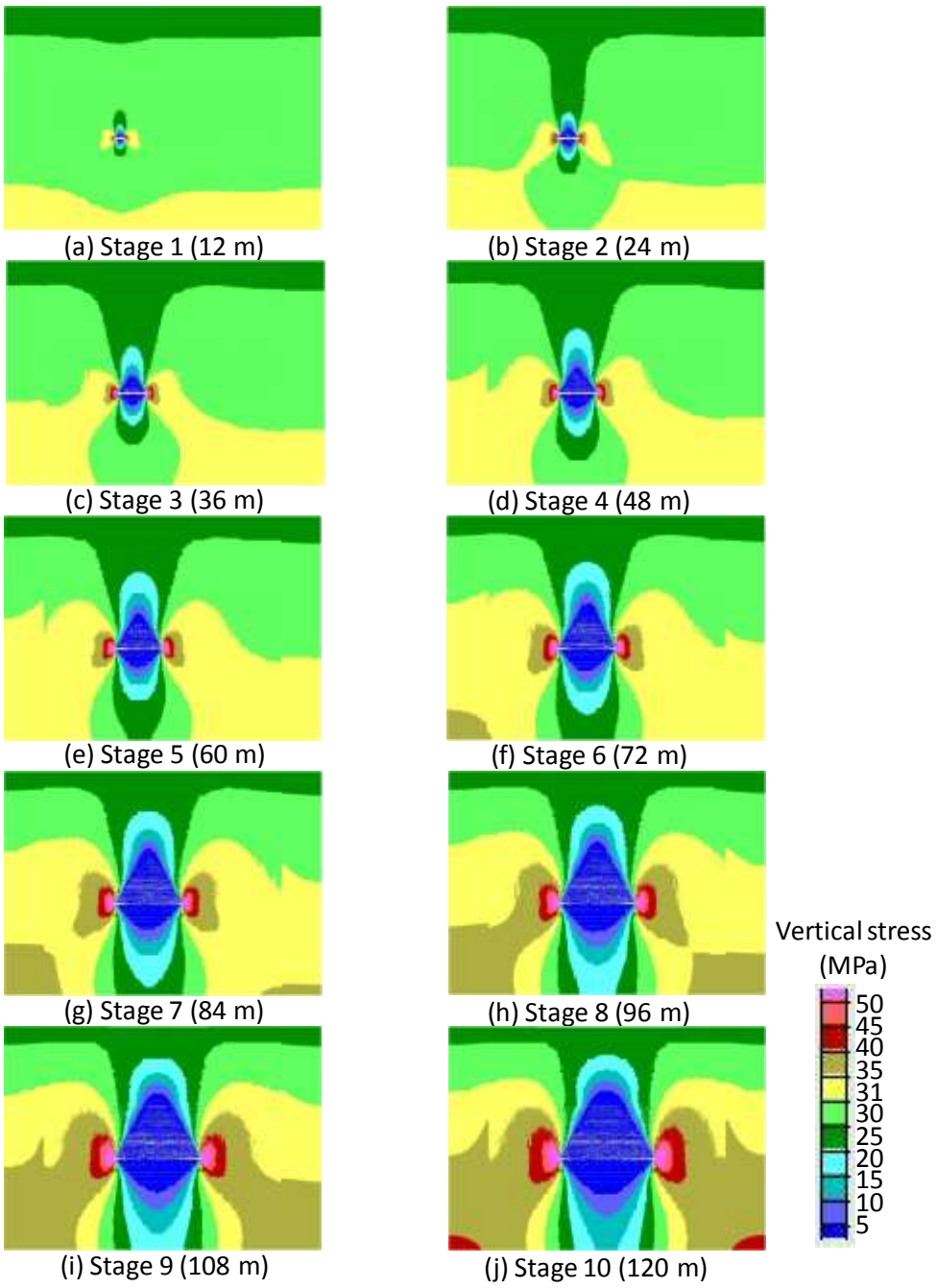

Fig. 7 Simulated vertical stress distribution with longwall face advance.

It should also be noted that the maximum values of the monitored vertical stress at all the 12 points is approximately 61.6 MPa, corresponding to 2.3 times the overburden stress. Traditional models have suggested that the peak vertical stress is in the order of four to six times the overburden stress [1,22]. The significant difference between the present results and previous models may be due to shear failure in the intact rock and along bedding planes which

reduces the load carrying capacity of the rock in the roof above the goaf. This effectively transfers the abutment peak stress away from the longwall and reduces its magnitude.

Fig. 9 shows the horizontal stress distribution around the longwall panel for the different mining stages. The extraction of coal causes horizontal stress relief in the immediate roof and floor and stress concentration in the un-mined coal. As the face advances, the extent and degree of both stress relief and stress concentration increases. The horizontal stress relief exhibits a pear-shaped region around the mined-out area, Fig. 9 (j).

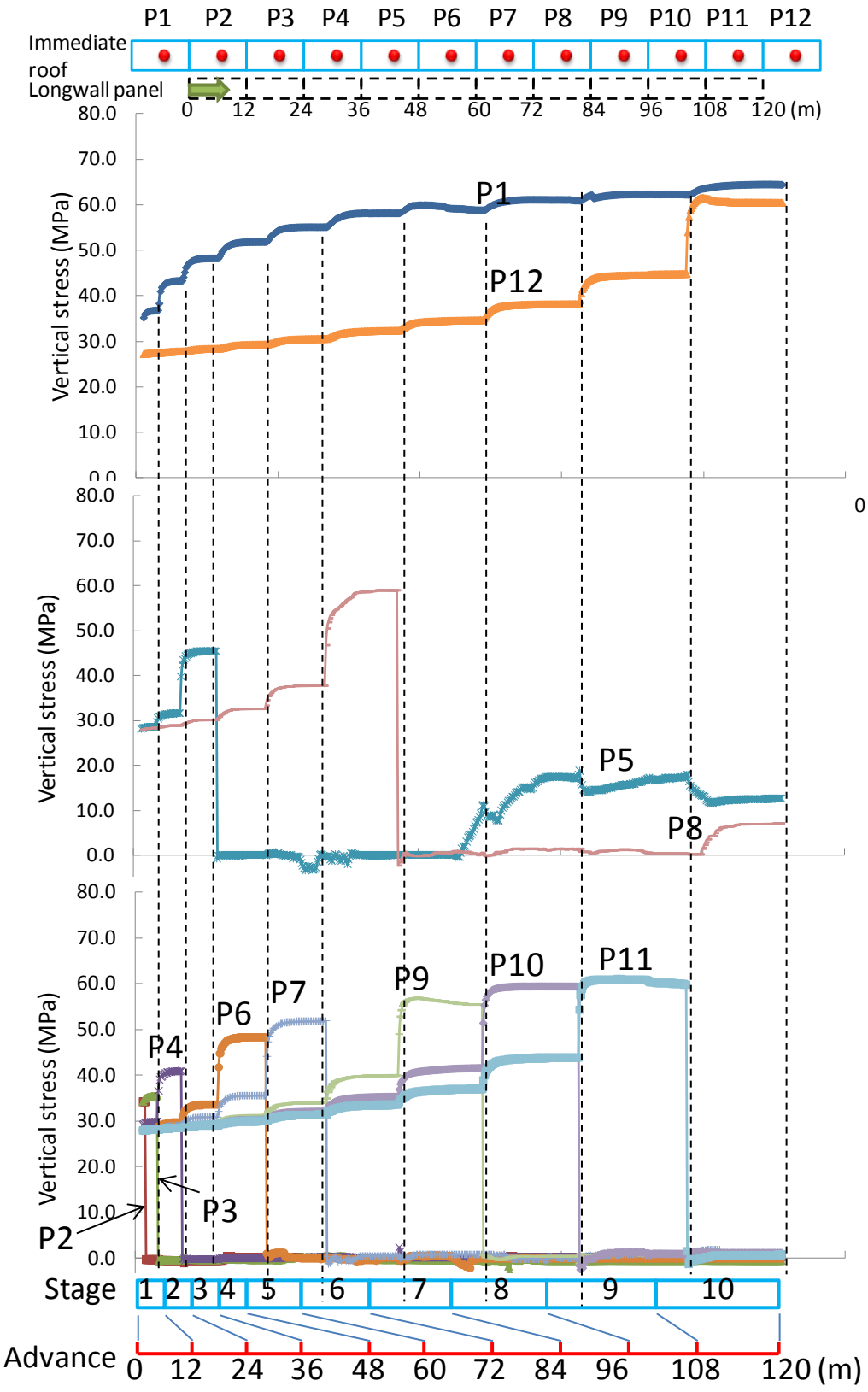

Fig. 8 ***Simulated vertical stress changes in the immediate roof above the goaf.***

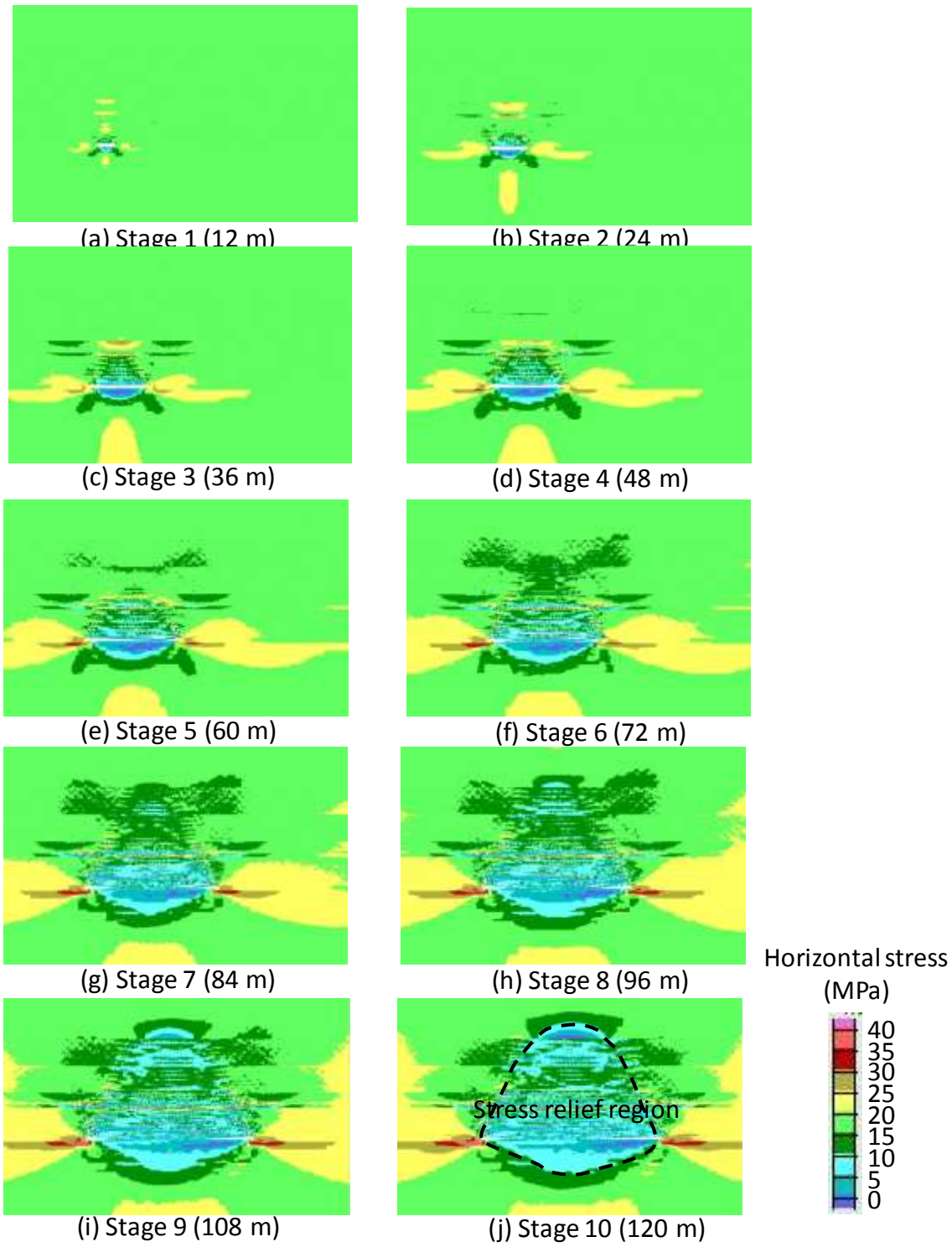

Fig. 9 ***Simulated distribution of horizontal stress as longwall face advances.***

3.3 Damage

A new approach is proposed to quantify the progressive failure of the longwall panel roof. Using the developed FISH function, the total length of shear and tensile cracks in different monitoring regions has been evaluated with face advance. A damage parameter *D* is proposed as:

$$D = \frac{L_s + L_t}{L_c} \times 100\% \quad (7.8)$$

In which, L_s is the total length of shear cracks, L_t is the total length of tensile cracks, and L_c is the total contact length.

For each mining stage, the *D* value is calculated at each monitoring region, and contour maps of damage at each mining stage drawn, Fig. 10. The extraction of the coal seam causes roof damage to start at the immediate roof and then propagate deeper above the main roof. In the first two stages, distinct damage (*D*>7%) is only observed in the immediate roof directly above the goaf. When the simulated face advances 36 m, distinct damage occurs at the H3 layer which comprises weak sandstone, even though distinct damage has not occurred across the entire 19-m thick immediate roof. Cracks can be observed approximately 50 m ahead of the face within the H3 layer. At mining stage 4, distinct damage occurs across the entire thick immediate roof. With continued face advance both the area of the damage regions and the damage parameter *D* increase. At the final modelled stage, the maximum *D* value occurs in the middle region of H3 layer when the *D* value is 88% (indicating that 88% of the contacts in the region have failed through either shear or tension).

A further evaluation of the roof damage is carried out by plotting the *D* value in the immediate roof against face advance, Fig. 11. In each monitoring region with the exception of Region 1, distinct damage initiates when the face is 12 m ahead and significantly deteriorates as the face passes. Limited further damage is observed with subsequent face advance. In the immediate roof, the maximum *D* value (65%) occurs in Region 25, which is located in the middle of the roof span. The *D* value decreases as the distance between the monitoring region and the middle Region 25 increases. The D values in all the monitoring regions except Region 1 are between 30% - 50%. In Region 1, the D value gradually increases as the face advances away from the region. Damage still develops when the face is over 84 m away.

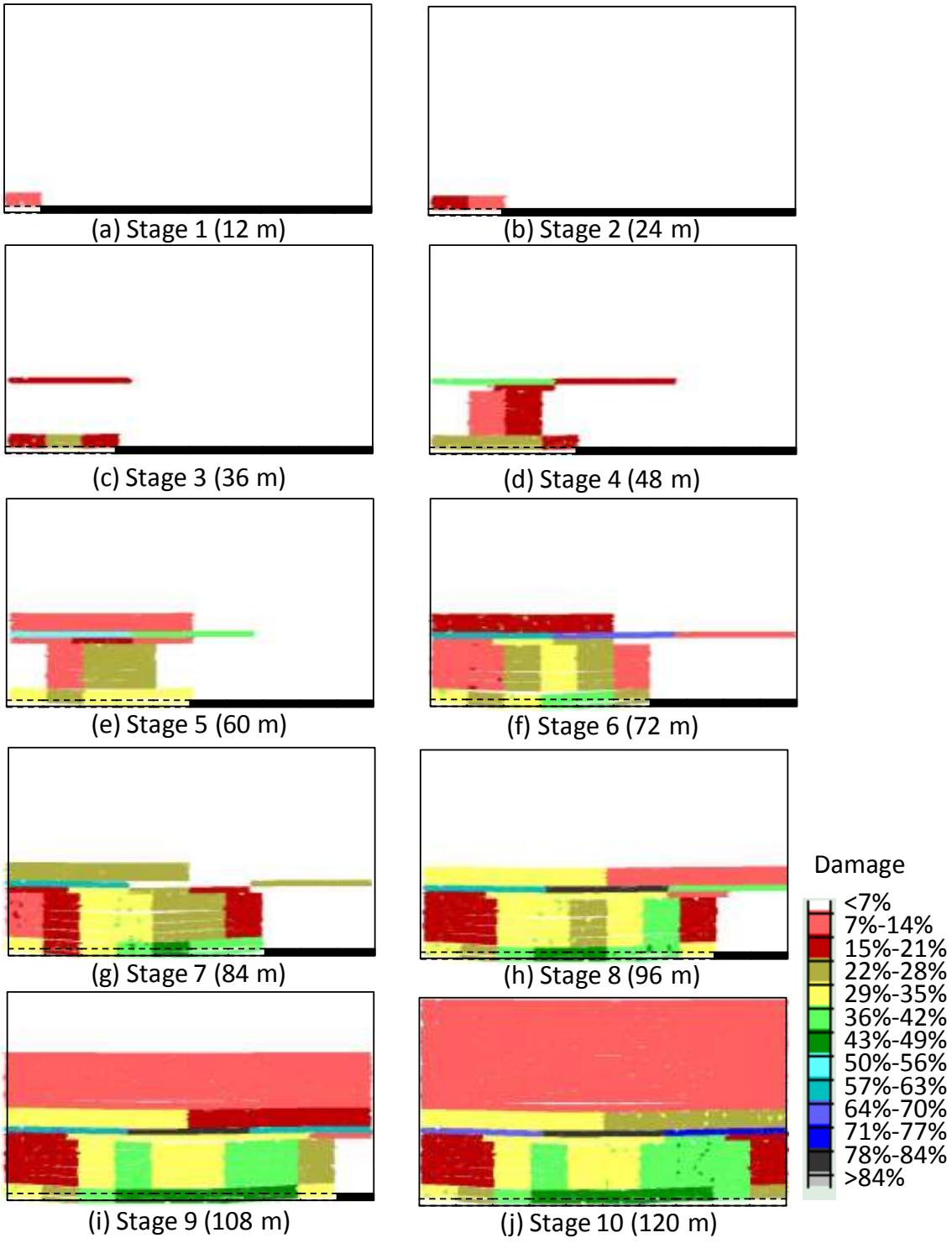

Fig. 10 ***Distribution of the damage parameter D in the longwall roof with face advance. The damage parameter D is defined in Eq (7.8).***

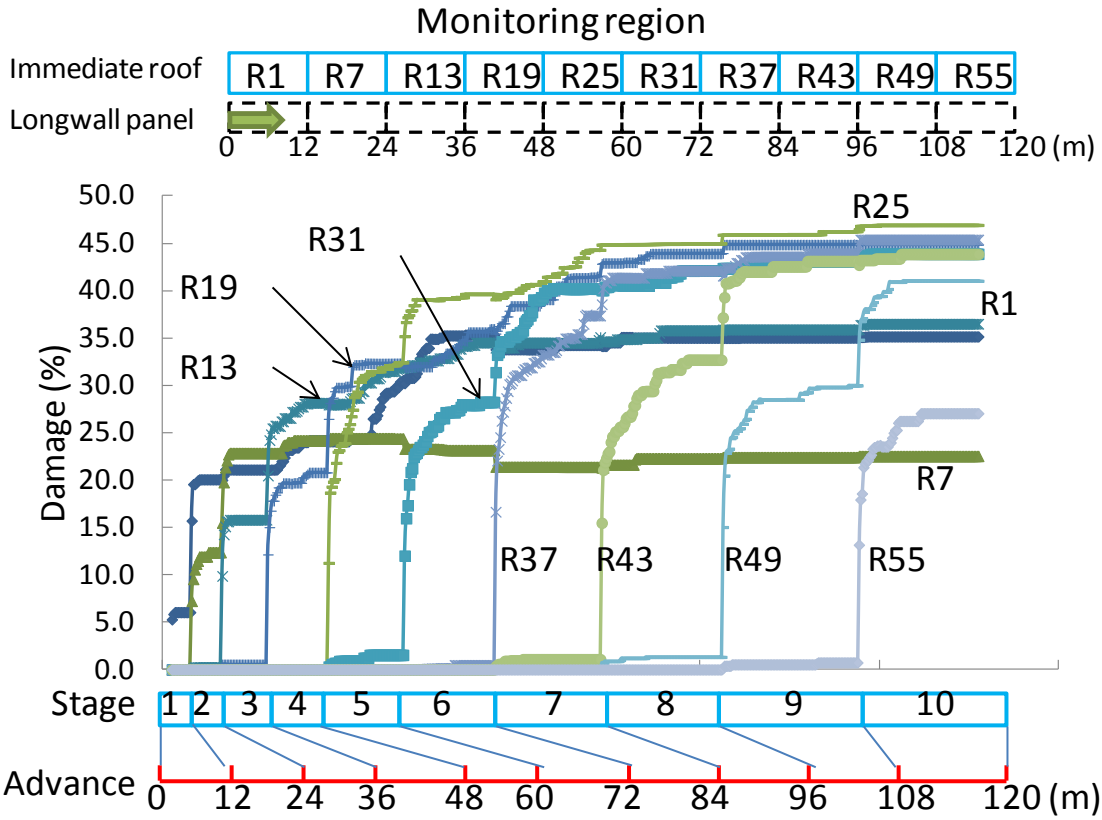

Fig. 11 ***Damage development in the immediate roof as the face advances.***

3.4 Failure mechanism

As discussed previously, the immediate roof fails in a beam bending failure mechanism, which is in agreement with field observations [19]. A field study using seismic moment tensor analysis by [6] showed that compressive shear, rather than tensile fracture, is the dominant failure mechanism in the roof. Their observations are confirmed by the present study which shows that shear cracking dominates tensile cracks in all model monitoring regions. Fig. 12 shows a contour plan of the ratio of shear cracking to tensile cracking in the roof. In all regions, the shear/tensile cracking ratio is greater than 5, indicating a predominant shear cracking mode. In layers H2 and H6 which are competent, the shear/tensile cracking ratio is greater than 36 with negligible simulated tensile cracking.

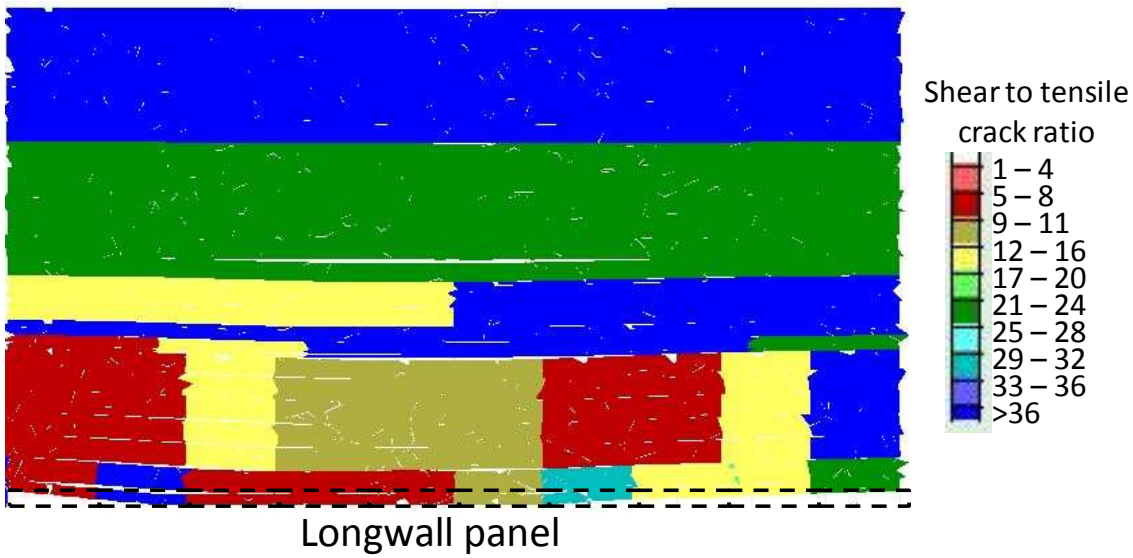

Fig. 12 Contour plan of the shear to tensile cracking ratio in the roof above the goaf.

3.5 Mechanism of Immediate roof collapse

The goaf can be categorized into four zones according to its collapse mechanism: i) cantilever zone in the back of the goaf, ii) compacted zone, iii) collapsed zone and iv) cantilever zone in the front of the goaf, as shown in Fig. 13. These zones can be identified according to the fracture mechanism. The cantilever zone in the back of the goaf comprises suspended beams with one end in the un-mined coal and the other in the compacted zone. It is characterized by a relatively lower damage (D<35%) (Fig. 10). The compacted zone forms when the immediate roof bends downward, caves and then is compacted. The collapsed zone forms when the immediate roof bends downward and caves, but is not compacted. As the face advances, the collapsed zone will subsequently be compacted. The cantilever zone in the front of the goaf is similar to the cantilever zone in the back of the goaf. The difference is that the cantilever zone in the front of the goaf will collapse and compact as the face advances whereas the cantilever zone in the back of the goaf is consolidated.

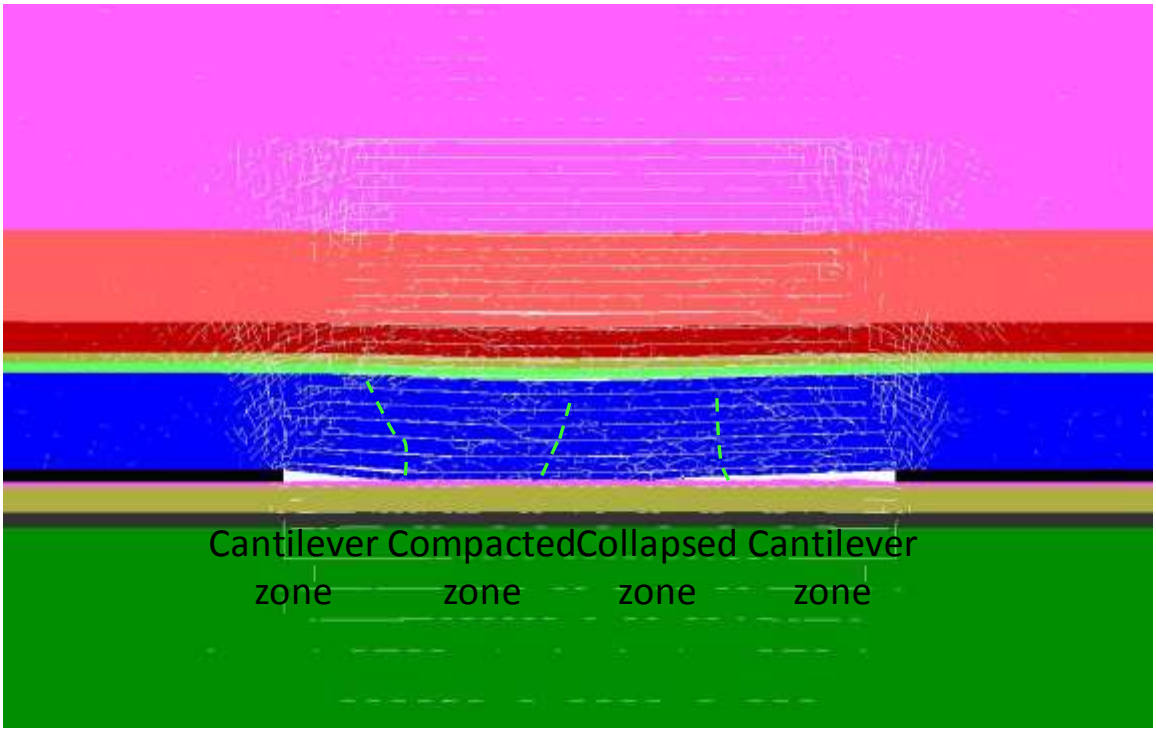

Fig. 13 ***Simulated immediate roof collapse pattern due to extraction of a panel in longwall coal mining.***

4 Effect of geological conditions on progressive longwall caving

4.1 Effect of bedding planes

Bedding planes have a significant influence on the fracture mechanism in the longwall roof. Fig. 14 presents the fracture patterns simulated in models with different bedding spacing. For the model where bedding planes are not taken into consideration, bed sliding along bedding plane and bending downward are ignored. The immediate roof does not act like beam and exhibits a massive collapse when the face advance is 108 m. It is suggested that bedding planes must be taken into consideration to achieve a realistic numerical simulation of progressive caving caused by longwall mining. Modelled bedding spacing has a considerable effect on the caving process. For example, for the model with a bedding spacing of 2.0 m, the immediate roof starts to cave as the face advances 48 m, when compared with an advance of 60 m for the model with a bedding spacing of 3.0 m.

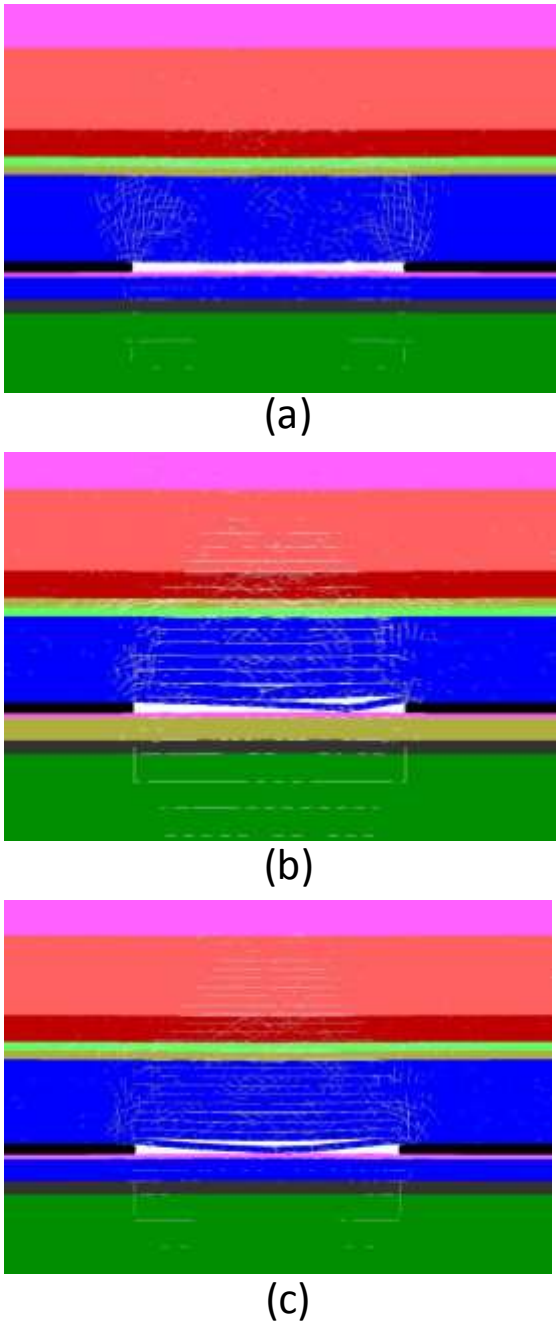

Fig. 14 ***Simulated fracture patterns in model (a) without bedding plane, (b) bedding spacing = 3.0 m, (c) bedding spacing = 2.0 m. The face advance is 60 m for all models shown.***

4.2 Effect of immediate roof strength

In the longwall panel in this study, the immediate roof is a 19-m thick massive sandstone with an intact compressive strength of 112 MPa. The numerical model shows that this strong roof does not cave until the face advances 60 m. The model was re-run with a softer immediate

roof by reducing the cohesion, tensile strength, normal and shear stiffness of contacts and Young's modulus of blocks by half and keeping all other parameters constant. The softer immediate roof, as expected, caves more readily when the face advance is 48 m (Fig. 15), in contrast to 60 m with the stronger roof. In addition, the soft immediate roof is more likely to be fractured and tends to relieve stress concentration caused by the extraction of the coal seam, Fig. 16. In the mined out area, increased vertical stress concentrations are more likely in the model with the soft immediate roof.

4.3 Effect of high horizontal stress

As mentioned previously, the longwall panel is subjected to a high horizontal stress, $\sigma_H = 39$ MPa and $\sigma_h = 18$ MPa and σ_h is parallel to the face advance direction. As the σ_H is in the out-of-plane model direction of the 2D model its effect on the panel is not captured. When the model is repeated with the σ_H parallel to the face advance direction it is found that the high horizontal stress has a significant effect on both the fracture pattern in the immediate roof and the stress distribution around the panel. Under the high horizontal stress, a bearing beam is formed in the strong roof layer H3, Fig. 17 (a). This bearing beam complements the "stress-shell" developed in the roof above the un-mined coal, forming an entire bearing arch around the goaf. This bearing arch bears and transfers the loads of overlying strata to the unmined area, forming a stress-released zone below it. The most significant influence of this high horizontal stress is that it changes the fracture mechanism in the immediate roof from bed bending failure to bed shear fracture, Fig. 17 (b). The bed shear fracture may lead to a massive collapse of the thick strong immediate roof.

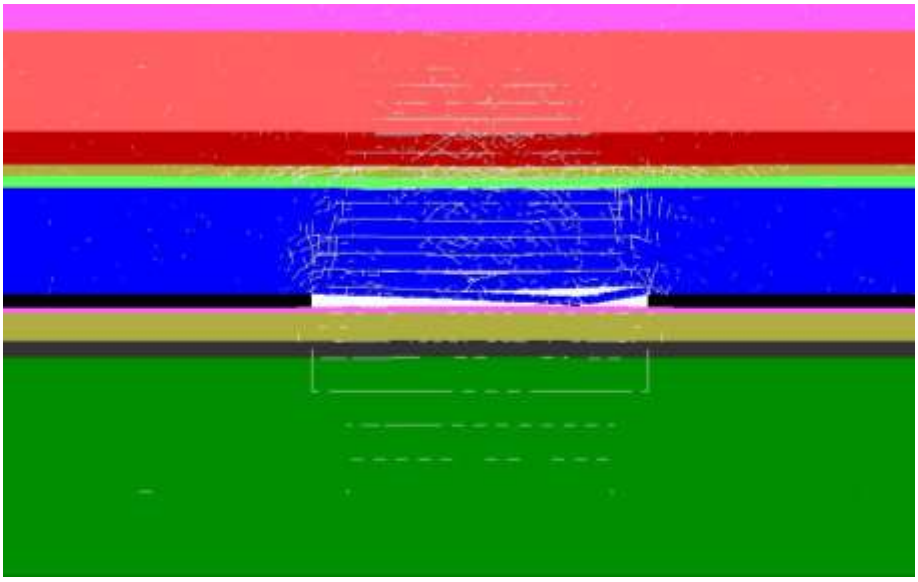

(a)

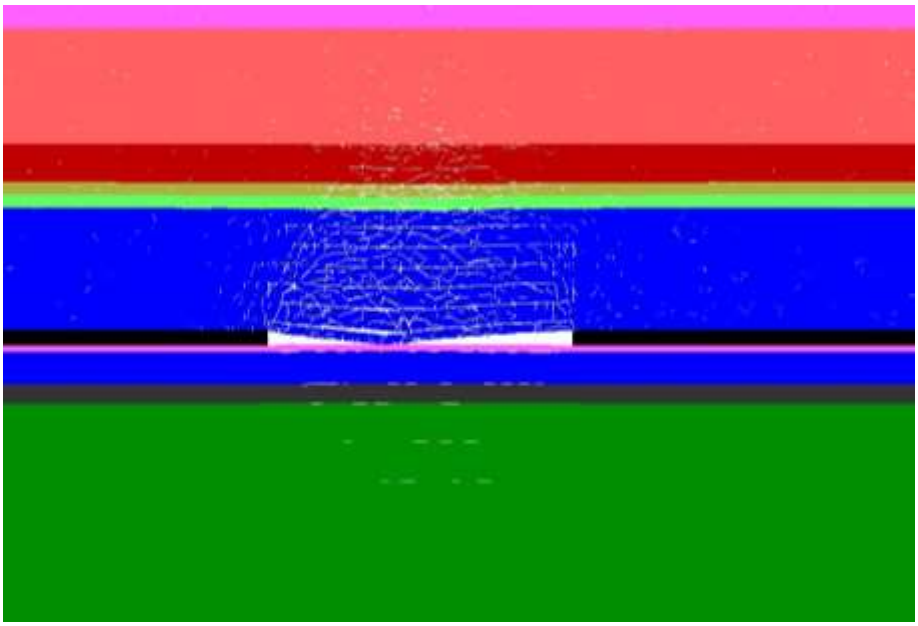

(b)

Fig. 15 ***Simulated fracture patterns in model with (a) strong roof which starts to cave as the face advances 60 m, (b) soft roof which starts to cave as the face advances 48 m.***

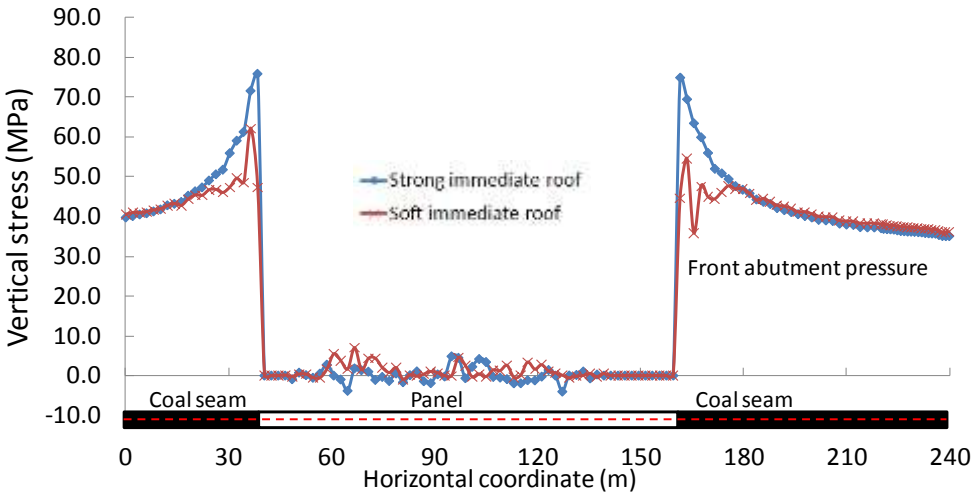

Fig. 16 ***Simulated vertical stress distribution along a horizontal line (dotted) in the longwall panel.***

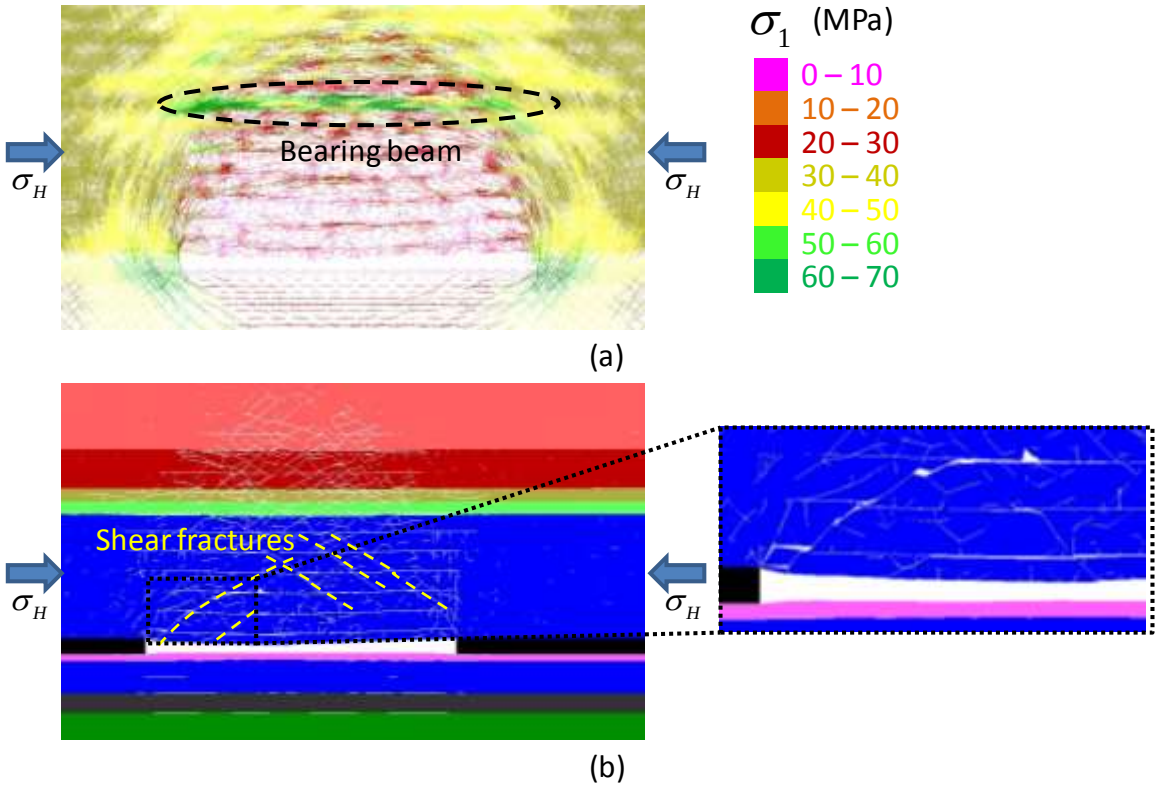

Fig. 17 ***Effect of high horizontal stress on stress distribution around the panel (a) and fracture mechanism in the immediate roof (b). The face advance is 60 m for models shown.***

5 Discussion

Extraction of a longwall panel induces stress changes and caving of the rock mass above the mined-out area through slipping along and opening of bedding planes, in addition to shear and tensile fracturing in the rock mass surrounding the panel. Many of these features are reproduced in the current numerical simulations using the new UDEC Trigon approach.

Investigation of the seismic events recorded in the field by previous researchers for the case study modelled have shown that the seismogenic zone can extend up to 100 m around the face [19]. In our numerical model, simulated cracks initiate 60 m in front of the face and cracking still occurs in the roof above the goaf when the face is 84 m away. The simulated results are in general agreement with the field observations, even though they underestimate the range of cracking around the face. This might be attributed to the fact that pore pressure was not taken into consideration in the current model. Water content and pore pressure have an influence on rock failure mechanism. A numerical study by [6] showed that a model incorporating fluid flow predicted shear failure extending to 40 m in advance of the face, compared with 10-15 from a model not considering fluid flow.

The simulated mining-induced stress changes reach up to approximately 80-90 m ahead the face. There is no stress change data available for the modelled case study so the current numerical results cannot be calibrated. However, Abdul-Wahed et al. found that the zone of stress changes in a coal mine at a similar depth reached approximately 50 m ahead of the actual face [23]. It should be noted that the range in mining-induced stress changes is related to numerous factors including geological and geotechnical conditions. Guo et al. carried out a field monitoring program at a deep (640-760 m) in a Chinese coal mine and suggested that the abutment stresses extend 300 m ahead of mining face, mining-induced fracturing occurs within 170 m behind the longwall face and extends up to 145 m above the goaf [24]. For the Gordonstone Mine in Australia, micro-seismic event locations showed that rock fracture or shear generally occurred within 30-50m but as much as 80 m, ahead of the face, and 100 m above or below the face [6].

The formation of the cantilever zone (Fig. 13) is due to the thick strong sandstone which is too competent to rupture. This is also the reason why the roof stays relatively intact (less damage than above strata, Fig. 12) as it caves into the opening. A model with weak immediate roof (1 MPa cohesion, 0.4 MPa tensile strength of the contact) shows that the roof ruptures or caves when the face advances 24 m, Fig. 18.

Fig. 18 ***Simulated fracture pattern in model with weak immediate roof. The roof ruptures when the face advances 24 m.***

6 Conclusions

In the present study, a new numerical approach has been used to simulate progressive caving caused by extraction of a longwall mining panel. The UDEC method with a proposed Trigon logic simulates the modelled roof as an assembly of triangular blocks bonded via contacts. Pre-existing fractures including bedding planes and cross joints have been incorporated within the model. Cracks formed through either shear or tension were monitored in different regions of the roof using a developed FISH function. Using this approach, a damage parameter D is introduced which makes it possible to quantitatively evaluate the roof failure mechanisms. The key results of this study are summarized as follows:

(1) The progressive caving caused by extraction of a longwall coal panel, including slipping along and opening of bedding planes and shear and tensile fracturing in the rock mass surrounding the panel, have been successfully reproduced in the present numerical simulation using the UDEC Trigon approach. The importance of pre-existing fractures including bedding planes and cross joints on modelled cave behavior is shown.

(2) The simulated cracks initiate 60 m in front of the face and 84 m behind the face. The simulated mining-induced stress changes can reach up to approximately 80-90 m ahead of the face. The numerical results are found to be in accordance with field observations.

(3) At the global scale, the thick immediate roof fails in a beam bending mechanism which is in agreement with field observation. At the local scale, compressive shear, rather than tensile fracture, is the dominate failure mechanism in the roof.

(4) High horizontal stress plays an important role in the progressive caving process. When the horizontal stress is the dominant stress over the vertical stress, the immediate roof fails in a beam shear fracture mechanism.

(5) The thick immediate roof caved in the goaf can be categorized into four zones according to the collapse mechanism. These are a cantilever zone in the back of the goaf, a compacted zone, a collapsed zone and a cantilever zone in the front of the goaf, Fig. 13.

It should be noted that the results are only part of 2D analyses which is a simple two-dimensional approximation of the actual three-dimensional longwall span and 3D complex stress field. Future work is needed to incorporate the proposed logic within 3D.

References

[1] Peng S. Coal Mine Ground Control (2nd edition). 2rd ed. Wiley, New York; 1986.

[2] Das SK. Observations and classification of roof strata behaviour over longwall coal mining panels in India 2000:585–97.

[3] Singh R, Singh TN. Investigation into the Behaviour of a Support System and Roof Strata During Sublevel Caving of a Thick Coal Seam. Geotech Geol Eng 1999;17:21–35.

[4] Xie GX, Chang JC, Yang K. Investigations into stress shell characteristics of surrounding rock in fully mechanized top-coal caving face. Int J Rock Mech Min Sci 2009;46:172–81.

[5] Islam MR, Hayashi D, Kamruzzaman ABM. Finite element modeling of stress distributions and problems for multi-slice longwall mining in Bangladesh, with special reference to the Barapukuria coal mine. Int J Coal Geol 2009;78:91–109.

[6] Kelly M, Luo X, Craig S. Integrating tools for longwall geomechanics assessment. Int J Rock Mech Min Sci 2002;39:661–76.

[7] Saeedi G, Shahriar K, Rezai B, Karpuz C. Numerical modelling of out-of-seam dilution in longwall retreat mining. Int J Rock Mech Min Sci 2010;47:533–43.

[8] Shabanimashcool M, Li CC. Numerical modelling of longwall mining and stability analysis of the gates in a coal mine. Int J Rock Mech Min Sci 2012;51:24–34.

[9] Singh GSP, Singh UK. A numerical modeling approach for assessment of progressive caving of strata and performance of hydraulic powered support in longwall workings. Comput Geotech 2009;36:1142–56.

[10] Singh GSP, Singh UK, Murthy VMSR. Applications of Numerical Modelling for Strata Control in Mines. Geotech Geol Eng 2010;28:513–24.

[11] Unver B, Yasitli NE. Modelling of strata movement with a special reference to caving mechanism in thick seam coal mining. Int J Coal Geol 2006;66:227–52.

[12] Whittles DN, Lowndes IS, Kingman SW, Yates C, Jobling S. Influence of geotechnical factors on gas flow experienced in a UK longwall coal mine panel. Int J Rock Mech Min Sci 2006;43:369–87.

[13] Coulthard MA. Applications of numerical modelling in underground mining and construction. Geotech Geol Eng 1999;17:373–85.

[14] Itasca Consulting Group Inc. UDEC (Universal Distinct Element Code), Version 4.1. Minneapolis: Itasca; 2011.

[15] Alehossein H, Poulsen BA. Stress analysis of longwall top coal caving. Int J Rock Mech Min Sci 2010;47:30–41.

[16] Kwaśniewski M. Numerical analysis of strata behavior in the vicinity of a longwall panel in a coal seam mined with roof caving. 1st Int. Flacdem Symp., vol. 07-08, Minneapolis, US: 2008, p. 12.

[17] Quang HD, Mitra R, Hebblewhite B. Effect of Seam Dip on Face Orientation of Longwall Top Coal Caving. 43rd Us Rock Mech. Symp. 4th Us-Can. Rock Mech. Symp., vol. 09-110, Asheville, USA: 2009, p. 9.

[18] Vakili A, Hebblewhite BK. A new cavability assessment criterion for Longwall Top Coal Caving. Int J Rock Mech Min Sci 2010;47:1317–29.

[19] Alber M, Fritschen R, Bischoff M, Meier T. Rock mechanical investigations of seismic events in a deep longwall coal mine. Int J Rock Mech Min Sci 2009;46:408–20.

[20] Hoek E, Brown ET. Practical estimates of rock mass strength 1997:1165–86.

[21] Rocscience. Rocscience Software products, DIPS, SWEDGE, SLIDE and PHASE2. Toronto: Rocsience Inc.; 2013.

[22] Whittaker BN. An appraisal of strata control practice 1974;134:9–22.

[23] Abdul-Wahed MK, Al Heib M, Senfaute G. Mining-induced seismicity: Seismic measurement using multiplet approach and numerical modeling. Int J Coal Geol 2006;66:137–47.

[24] Guo H, Yuan L, Shen B, Qu Q, Xue J. Mining-induced strata stress changes, fractures and gas flow dynamics in multi-seam longwall mining. Int J Rock Mech Min Sci 2012;54:129–39.